

Finger Vein & Texture Recognition Using Score Level Fusion And 2-D Gabor Filter For Human Identification

Diptanu Bhowmik

(Regd. No. 3188113)

Department Of Ece, M.E Embedded System, Sathyabama University, Chennai-119, Tamil Nadu, India

ABSTRACT

The paper presents a new approach to improve the performance of finger-vein identification systems presented in the literature. The proposed system simultaneously acquires the finger-vein and low-resolution fingerprint images and combines these two evidences using a novel score-level combination strategy. We examine the previously proposed finger-vein identification approaches and develop a new approach that illustrates its superiority over prior published efforts. We develop and investigate two new score-level combinations, i.e., holistic and nonlinear fusion, and comparatively evaluate them with more popular score-level fusion approaches to ascertain their effectiveness in the proposed system.

Keywords – Fingerprint Recognition, Finger-Vein Recognition, Fusion, Hand Biometrics

I. INTRODUCTION

Automated human identification using physiological and/or behavioural characteristics, biometrics, is increasingly mapped to new civilian applications for commercial use. The tremendous growth in the demand for more user-friendly and secured biometrics systems has motivated researchers to explore new biometrics features and traits. The anatomy of human fingers is quite complicated and largely responsible for the individuality of fingerprints and finger veins. The high individuality of fingerprints has been attributed to the random imperfections in the friction ridges and valleys, which are commonly referred to as minutiae or level-2 fingerprint features. The acquisition of such minutiae features typically requires imaging resolution higher than 400 dpi. The conventional level-1 fingerprint features, which illustrate macro finger details such as ridge flow and pattern type, can be extracted from the low-resolution fingerprint images. Such features are useful for fingerprint classification, although the commercially available automated fingerprint identification systems barely utilize such level-1 features. The utility of such

features, which can be more conveniently be acquired from the low-resolution (webcam) images or at a distance, deserves attention for its possible use in personal identification for civilian and/or forensic applications. The images at such low resolution typically illustrate friction creases and also friction ridges but with varying clarity. Several biometrics technologies are susceptible to spoof attacks in which fake fingerprints, static palm prints, and static face images can be successfully employed as biometric samples to impersonate the identification. Therefore, several liveness countermeasures to detect such sensor-level spoof attacks have been proposed, e.g., finger response to electrical impulse, finger temperature and electrocardiographic signals, time-varying perspiration patterns from fingertips, and a percentage of oxygen-saturated hemoglobin in the blood. Despite the variety of these suggestions, only a few have been found suitable for online fingerprint identification, and these techniques require close contact of respective sensors with the fingers, which makes them unsuitable for unconstrained finger images or when the presented fingers are not in close proximity with the sensors

II. BLOCK DIAGRAM AND EXPLANATION

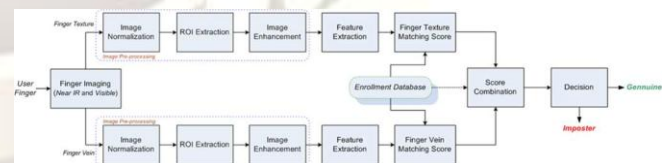


Fig. 1. Block diagram for personal identification using simultaneous finger vein and finger texture imaging.

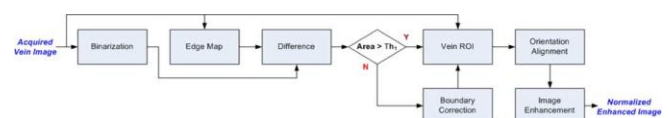


Fig. 3. Block diagram illustrating key steps employed for the preprocessing of acquired finger-vein images.

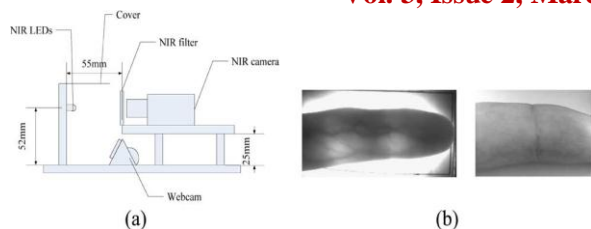


Fig. 2. (a) Unconstrained finger identification using near-infrared camera and webcam imaging. (b) Simultaneously acquired image samples from the imaging device.

The block diagram of the proposed system is shown in Fig. 1.

The fingers presented for the identification of subjects are simultaneously exposed to a webcam and an infrared camera, as illustrated from the device of our imaging device in Fig. 2(a).

The dorsal side of a finger is exposed to the near-infrared frontal surface illuminators, using light-emitting diodes whose illumination peaks are at a wavelength of 850 nm, whereas the frontal surface entirely remains in the contactless position with both of the imaging cameras. Although our imaging system is unconstrained, i.e., it does not use any pegs or finger docking frame, it may not be designated as completely touchless. This is because the user often partially or fully touches the finger dorsal surface with the white diffusion background, which holds the infrared illuminators beneath. The finger-vein and finger texture images are simultaneously acquired using the switching device/ hardware that can switch the infrared illumination at a fast pace. Fig. 2(b) shows a typical image samples acquired from our device from a left index finger. The near-infrared illumination incident on the finger dorsal surface is absorbed by the branches of arteries, veins, and hemoglobin in the blood. However, the scattering and the absorption coefficients of biotissue is significantly different to that of blood for the infrared illumination. The higher scattering coefficient results in more path changes of incident-inferred illumination from the blood than those resulting from the surrounding tissues. Therefore, it is scattering from infrared illumination, rather than absorption, that dominates and results in a darker appearance of finger-vein patterns. The acquired finger-vein and finger texture images are first subjected to preprocessing steps, which automatically extract the region-of-interest (ROI) images while minimizing the translational and rotational variations. These steps are detailed in Sections III and V for the finger-vein and finger texture images, respectively. The enhanced and normalized ROI images are employed to extract features and then generate matching scores similar with a conventional biometrics system. The

combined matching scores are employed to authenticate the user.

FINGER-VEIN IMAGE PREPROCESSING

The acquired finger images are noisy with rotational and translational variations resulting from unconstrained (peg-free) imaging. Therefore, the acquired images are first subjected to preprocessing steps (see Fig. 3) that include: 1) segmentation of ROI, 2) translation and orientation alignment, and 3) image enhancement to extract stable/reliable vascular patterns. Each of the acquired finger-vein images is first subjected to binarization, using a fixed threshold value as 230, to coarsely localize the finger shape in the images. Some portions of background still appear as connected to the bright finger regions, predominantly due to uneven illumination. The isolated and loosely connected regions in the binarized images are eliminated in two steps: First, the Sobel edge detector is applied to the entire image, and the resulting edge map is subtracted from the binarized image. Subsequently, the isolated blobs (if any) in the resulting images are eliminated from the area thresholding, i.e., the eliminating number of connected white pixels being less than a threshold.

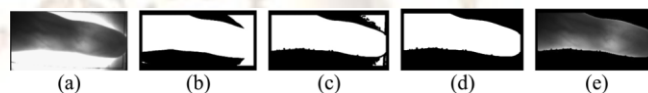


Fig. 4. Extraction of ROI from finger vein images. (a) Acquired image sample. (b) Binarized image. (c) Edge map subtracted from (b). (d) ROI mask from the image in (c) and the ROI finger vein image.

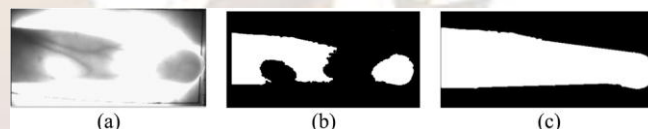


Fig. 5. (a) Acquired finger vein image. (b) ROI mask from (a). (c) ROI mask after refinement

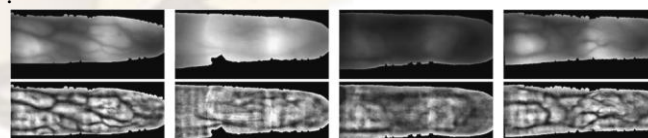


Fig. 6. Finger vein images after ROI localization (upper row) and the corresponding images after enhancement (lower row).

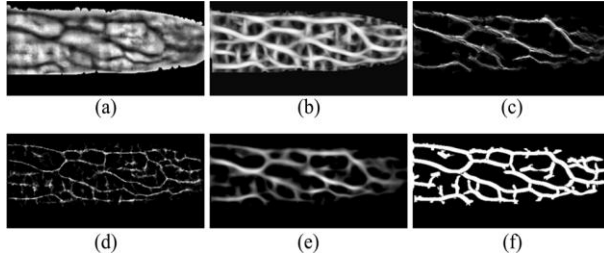


Fig. 7. Sample results from different feature extraction methods. (a) Enhanced finger-vein image. (b) Output from the matched filter. (c) Output from repeated line tracking. (d) Output from the maximum curvature. (e) Output from Gabor filters. (f) Output from morphological operations on (e)

A. Coarse Finger Localization and Alignment

The extraction of the ROI discussed above works well in most cases. However, there are some low-quality images that illustrate portions of the finger, whereas some images present largely broken finger boundaries.² Therefore, such images require further processing. As shown in Fig. 5, such images are identified from the number of white pixels (smaller than the threshold). The upper and lower boundaries of the finger can be used to estimate the slope of finger shape boundaries. First, an initial point of the finger boundary from the left end is selected, and then, another boundary point on the same side is sampled at a distance away from the starting point. The slope computed from using pair of these points is used to approximate the missing finger boundary. The selection of sampling distance plays an important role in the accuracy of such approximation; overdue short distance may not represent the entire trends in the slope, whereas large distance introduces bias and generates poor results. The key purpose of finger boundary estimation is to ensure that the rotational alignment of finger will be carried out more precisely.

The orientation of finger-vein images is estimated from the orientation of binarizedmask [see Figs. 4(d) or 5(c)], which is generated from the localization of ROI

B.FINGER VEIN IDENTIFICATION

➤ Image normalization:

Normalization is a process that changes the range of pixel intensity values. In this, the image is subjected to binarization with threshold value of 230. Sobel edge detector is applied to the image to remove background portions connected to it. Eliminating the number of connected white pixels being less than a threshold, to obtain the binary mask. Binarization is a method of transforming grayscale image pixels into either black or white pixels by

selecting a threshold. The process can be fulfilled using a multitude of techniques. Fingerprint Image Binarization is to transform the 8-bit Gray fingerprint image to a 1-bit image with 0-value for ridges and 1-value for furrows. After the operation, ridges in the fingerprint are highlighted with black color while furrows are white. A locally adaptive binarization method is performed to binarize the fingerprint image

➤ ROI extractor:

In the finger images, there are many unwanted regions (that cannot be taken for analysis) has been removed by choosing the interested area in that image. The useful area is said to be "Region of Interest". The obtained binary mask is used to segment the ROI (Region Of Interest) from the original finger-vein image. The orientation of the image is determined to remove the low quality images that present in finger vein image. This orientation is used for the rotational alignment of the ROI in vein image.

➤ Image enhancement:

The acquired image is thin and it is not clear. So the image is enhanced by using bicubic interpolation for better visualization. Fingerprint Image enhancement is to make the image clearer for easy further operations. Since the fingerprint images acquired from sensors or other Medias are not assured with perfect quality, those enhancement methods, for increasing the contrast between ridges and furrows and for connecting the false broken points of ridges due to insufficient amount of ink, are very useful for keep a higher accuracy to fingerprint recognition.

B. FINGER TEXTURE IMAGE IDENTIFICATION:

➤ Localization and Normalization:

In texture preprocessing, Sobel edge detector is used to obtain the edge map and localize the finger boundaries. This edge map is isolated with noise and it can be removed from the area threshold. From this slope is estimated to automatically localize a fixed rectangular area. This slope is used to automatically localize a fixed rectangular area, which begins at a distance of 20 pixels from the upper finger boundary and is aligned along its estimated slope. We extract a fixed 400 160 pixel area, at a distance of 85 and 50 pixels, respectively, from the lower and right boundaries, from this rectangular region. This 400 160 pixel image is then used as the finger texture image for the identification.

➤ Image Enhancement:

In image enhancement, finger texture image is subjected to median filtering to eliminate the impulsive noise. The resulting images have low contrast and uneven illumination. Therefore obtain the background illumination image from the average of pixels in 10x10 pixel image subblocks and bicubic interpolation. The resulting image is subtracted from the median-filtered finger texture image.

➤ **Finger texture image feature extraction:**
Gabor filter is used for finger texture image feature extraction. Gabor filters optimally capture both local orientation and frequency information from a fingerprint image. By tuning a Gabor filter to specific frequency and direction, the local frequency and orientation information can be obtained. The normalized and enhanced finger texture image have varying thickness and clarity on the topological connections. The finger texture features can be extracted by using Gabor filter.

D.GABOR FILTER

Gabor filters are directly related to Gabor wavelets, since they can be designed for number of dilations and rotations. However, in general, expansion is not applied for Gabor wavelets, since this requires computation of biorthogonal wavelets, which may be very time-consuming. Therefore, usually, a filter bank consisting of Gabor filters with various scales and rotations is created. The filters are convolved with the signal, resulting in a so-called Gabor space. This process is closely related to processes in the primary visual cortex. The Gabor space is very useful in e.g., image processing applications such as iris recognition and fingerprint recognition.

A Gabor filter can be viewed as a sinusoidal plane of particular frequency and orientation, modulated by a Gaussian envelope.

$$G(x,y) = s(x,y) g(x,y)$$

where $s(x,y)$ is complex sinusoid and $g(x,y)$ is 2D gaussian envelope

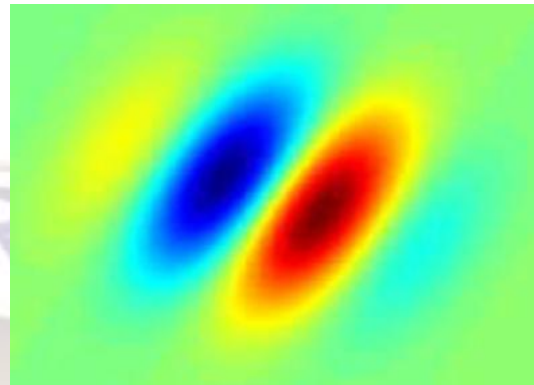
$$s(x,y) = \exp [-j2\pi (\mu_0 x + \nu_0 y)].$$

$$g(x,y) = \frac{1}{\sqrt{2\pi\sigma_x\sigma_y}} \exp \left[-\frac{1}{2} \left(\frac{x^2}{\sigma_x^2} + \frac{y^2}{\sigma_y^2} \right) \right]$$

Here is the formula of a complex Gabor function in space domain

$$g(x,y) = s(x,y)w_r(x,y)$$

Where $S(x,y)$ is a complex sinusoid, known as the carrier, and $W_r(x,y)$ is a 2-D Gaussian shaped function, known as the envelope.



ENVELOPE OF 2-D GABOR FILTER

The complex sinusoid carrier:

The complex sinusoid is defined as follows,

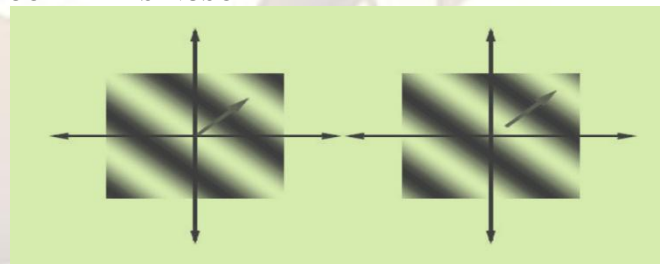
$$s(x,y) = \exp (j(2\pi(u_0x + v_0y) + P))$$

The real part and imaginary part of this sinusoid are

$$Re(s(x,y)) = \cos(2\pi(u_0x + v_0y) + P)$$

$$Im(s(x,y)) = \sin(2\pi(u_0x + v_0y) + P)$$

THE REAL AND IMAGINARY PARTS OF A COMPLEX SINUSOIDAL



The Gaussian envelope:

The Gaussian envelope looks as follows:

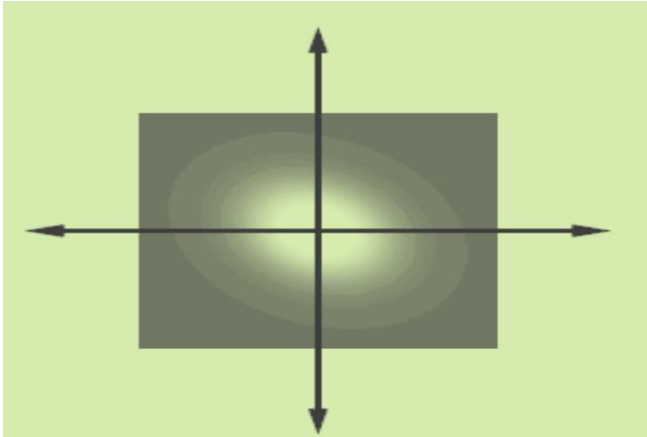
$$\omega_r(x,y) = K \exp (-\pi(a^2(x-x_0)_r^2 + b^2(y-y_0)_r^2))$$

where (X_0, Y_0) is the peak of the function, a and b are scaling parameters of the Gaussian, and the r subscript stands for a rotation operation such that

$$(x - x_o)_r = (x - x_o)\cos\theta + (y - y_o)\sin\theta$$

$$(y - y_o)_r = -(x - x_o)\sin\theta + (y - y_o)\cos\theta$$

GAUSSIAN ENVELOPE



Temporal and spatial Gabor example:

The Temporal Gabor Filter shown here is based on a sinusoid with a period of 56msec modified by a Gaussian envelope with a Standard Deviation of 22.4msec (Resolution= 4msec). The phase difference between the sinusoid and the Gaussian is 0. The spatial Gabor filter is based on a sinusoidal plane wave with a period of 2.8mm and a 2-D Gaussian with a Standard Deviation 1.12mm (resolution=0.2mm, phase=0). The difference of Gaussians filters represents the difference between a pair of 2-D Gaussians with Standard Deviations of 0.6mm and 0.9mm. In this case, the narrower Gaussian was positive and the broader was negative, so the filter has an “on-center” shape.

TEMPORAL AND SPATIAL GABOR FILTER

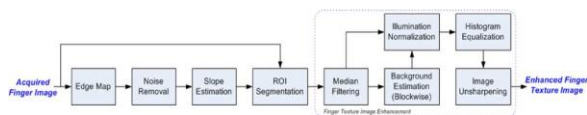
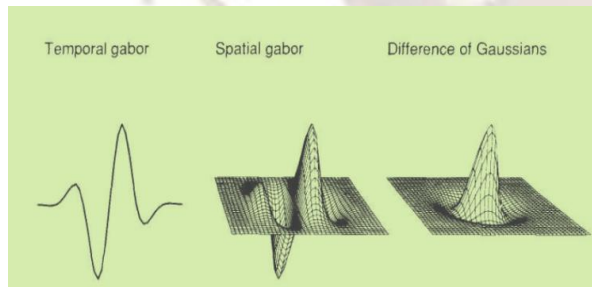


Fig. 8. Block diagram illustrating key steps employed for the preprocessing of acquired finger texture images from a webcam.

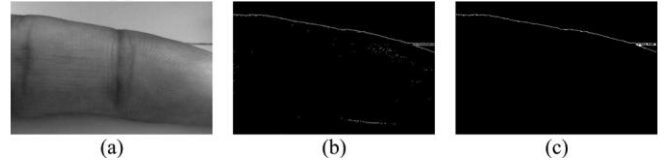


Fig. 9. Localization of finger texture regions. (a) Original image. (b) edge map. (c) Image after area thresholding.

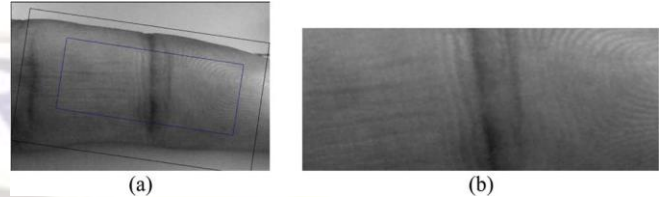


Fig. 10. Illustration of the localized rectangular region for (a) finger texture image and (b) segmented finger texture image.

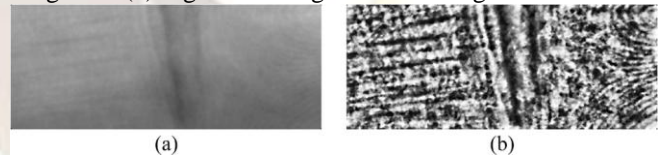


Fig. 11. (a) Median-filtered finger texture image. (b) Enhanced image using unsharpening .

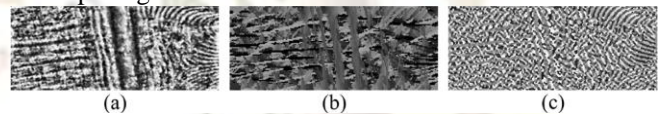


Fig. 12. (a) Enhanced finger texture image. Corresponding feature map using (b) LRT and (c) Gabor filters.

III. FIGURES AND TABLES

TABLE 1: PERFORMANCE FROM FINGER-VEIN MATCHING WITH VARIOUS APPROACHES (WITHOUT A MASK)

Approach	Index Finger	Middle Finger	Index and Middle Finger
Even Gabor with Morphological	7.14%	12.39%	9.31%
Repeated line tracking [5]	15.28%	18.59%	16.70%
Maximum curvature [6]	15.41%	18.06%	16.61%
Matched filter	8.60%	11.87%	10.00%
Even Gabor	6.50%	10.12%	8.10%

TABLE 2: PERFORMANCE FROM FINGER-VEIN MATCHING WITH VARIOUS APPROACHES (WITH A MASK)

Approach	Index Finger	Middle Finger	Index and Middle Finger
Even Gabor with Morphological	3.33%	6.99%	4.91%
Repeated line tracking [5]	15.60%	18.18%	16.43%
Maximum curvature [6]	10.96%	11.08%	10.99%
Matched filter	4.84%	7.81%	5.31%
Even Gabor	3.82%	7.08%	4.61%

TABLE 3:

PERFORMANCE FROM FINGER TEXTURE MATCHING WITH VARIOUS APPROACHES

Approach	Index finger	Middle Finger	Index and Middle finger
LRT (global)	6.58%	8.58%	7.79%
LRT (local)	5.50%	7.91%	6.86%
LRT (global with rotation)	3.95%	6.92%	5.75%
LRT (local with rotation)	4.49%	7.08%	5.73%
CompCode [43]	13.92%	15.73%	14.76%

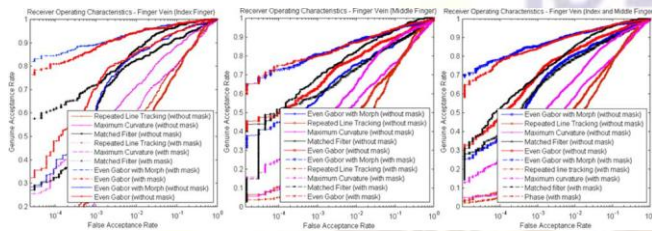


Fig. 13. ROCs from finger-vein images (experiment A).

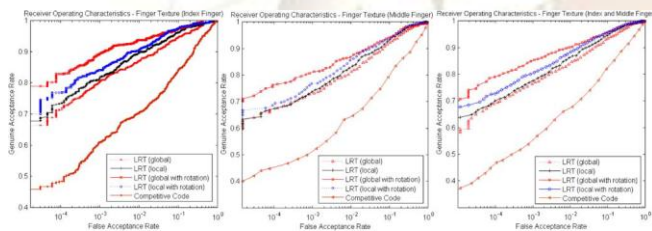


Fig. 14. ROCs from finger texture images (experiment A).

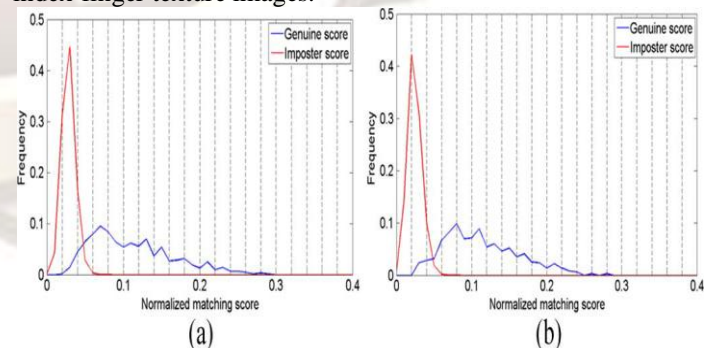
Experiment

The key objective of this set of experiments was to ascertain the robustness of various algorithms when the finger image data from both sessions was employed. The time span between data/imaging sessions is likely to introduce variations in the images, mainly from temporal changes (if any, in vein and/or texture patterns) and/or pose variations resulting from unconstrained finger imaging. First, six finger images and six finger texture images acquired during the first imaging session were employed to build up the training set, whereas the corresponding 12 images acquired during the second session are used as testing/validating data to ascertain the performance. Therefore, the number of genuine scores is 630 (105 6), and the number of imposter scores is 65 520 for each of the finger-vein and finger texture matching. Second, the different fingers from the same subjects were treated as belonging to different classes (i.e.,

210 classes), and the performance was also ascertained using the same protocol as mentioned before, which resulted in 1260 (2106) genuine and 263 340 imposter scores for each of the verification cases. Parameter was fixed as 12 for all the experiments in this paper. The experimental results from various approaches (discussed in Sections IV and V) using the equal error rate (EER) are summarized in Tables I–III, respectively, for vein and texture matching. The receiver operating characteristics (ROCs) for the corresponding performances are illustrated in Figs. 13 and 14. The experimental results from Tables I and II suggest significant improvement in the performance (over 40% in EER) from the proposed use of masks for all the approaches, except for the repeated line tracking. The plausible reason for such performance improvement by a masked matching scheme lies in the effective elimination of false/erroneous matches outside the finger boundaries. In addition, the use of the masks makes use of part of finger shape information; therefore, the matching is more discriminable. It can also be ascertained from Table II and Fig. 2 that the proposed scheme using even Gabor filters with the morphological processing achieves the best performance among all the approaches considered in this paper. Particularly, the success

of them rphological approach may contributed by emphasizing on the shape/structure features of the vein (see Section X-A) since, after this procedure, all the vein lines/curves are processed to similar width. The repeated line tracking and the maximum curvature approaches do not perform well.

Fig. 15. Genuine and imposter score distribution using enriched training samples from (a) local matching scheme, and (b) global matching scheme using index-finger texture images.



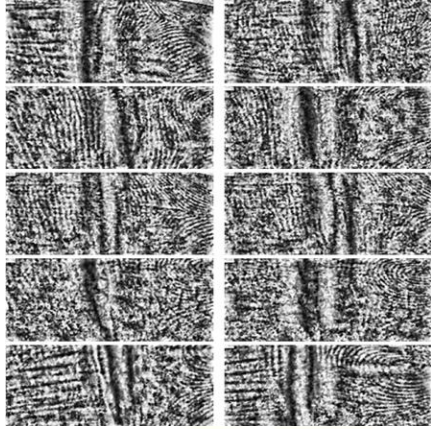


Fig. 16. Typical finger texture images after normalization to illustrate inherent translation and rotation. The images in each row are from the same subject

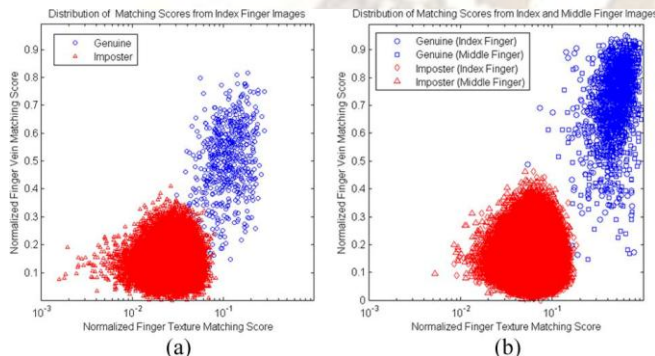


Fig.19. Distribution of finger-vein and finger texture matching scores from
 (a) index finger in experiment A and from (b) index and middle fingers in experiment B..

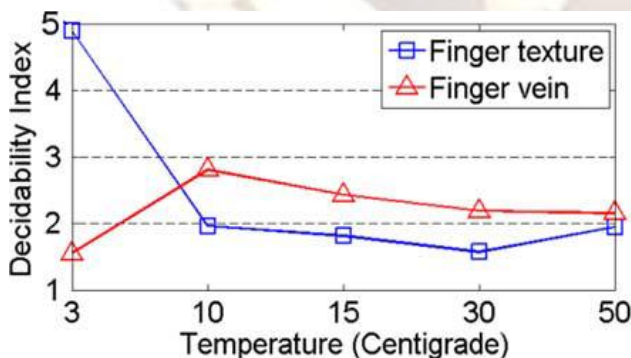


Fig. 20. Variation of the decidability index with temperature on sample finger images.

IV.CONCLUSION

In this paper, it presents a complete and fully automated finger image matching framework by

simultaneously utilizing the finger surface and finger subsurface features, i.e., from finger texture and finger-vein images .We presented rigorous experimental results on the database of 6264 images acquired from 156 subjects, over a period of 11 months, to illustrate the significant improvement in the performance than those using conventional finger-vein identification approaches. Second, we presented a new algorithm for the finger-vein identification, which can more reliably extract the finger-vein shape features and achieve much higher accuracy than previously proposed finger-vein identification approaches. Our finger-vein matching scheme (see Section IV-A-3) works more effectively in more realistic scenarios and leads to a more accurate performance, as demonstrated from the experimental results.

Third, the proposed and investigated two new score-level combination approaches, i.e., nonlinear and holistic, for effectively combining simultaneously generated finger-vein and finger texture matching scores. The nonlinear approach consistently performed better than other promising approaches, i.e., average, product, weighted sum, Dempster–Shafer, and Likelihood -ratio approaches, considered in this paper. Fourth, we examined a complete and fully automated approach for the identification of low-resolution finger surface/texture images for the performance improvement. This investigation and the obtained results are significant as they point toward the utility of touchless images acquired from the webcam for personal identification and its extension for other utilities such as mobile phones, surveillance cameras, and laptops. Finally, the availability of the acquired database from this paper for the benchmarking/comparison will help further the research efforts in this area. Currently, there is no publicly available database for the performance comparison and research efforts on finger-vein identification. The availability of this database, acquired in more realistic conditions, will compliment similar efforts, .

The unconstrained finger surface imaging employed in this paper utilized low-resolution images with varying clarity, and our attempts to extract stable minutiae features were not successful. Therefore, we relied on extracting texture like features to achieve reliable identification, and the rigorous experimental results presented in Section IX have suggested its promises. However, such features may not have high individuality in very large populations, or yet to be ascertained, to compete with more stable minutiae features employed in the conventional fingerprint identification systems. Despite possible reservation on the promises for

large-scale performance from such features, our experimental results have suggested that the investigated approach can be certainly useful for personal identification in small- and medium-size population. Importantly, such information can be highly useful when the quality of finger-vein patterns in an individual is weak or unstable. Although a lot remains to be done, our results to date indicate that the proposed combination of finger-vein and finger surface features constitutes a promising addition to the biometrics-based personal identification. The proposed algorithm is an alternative to currently employed finger-vein identification approaches that do not take advantage from the cross-level image measurements. Further improvement in the performance from the proposed approaches using feature discretization and image quality measurements is expected and is suggested for the further work on the large-scale finger image databases.

REFERENCES

[1] *Encyclopedia of Biometrics*, S. Z. Li, Ed., New York: Springer- Verlag, 2009.

- [2] E. C. Lee and K. R. Park, "Restoration method of skin scattering blurred vein image for finger vein recognition," *Electron. Lett.*, vol. 45, no. 21, pp. 1074–1076, Oct. 2009.
- [3] J.-D.Wu and S.-H. Ye, "Driver identification using finger-vein patterns with Radon transform and neural network," *Expert Sys. And Appl.*, vol. method," U.S. Patent 20 100 080 422 A1, Apr. 1, 2010
- [4] Feature extraction of finger vein patterns based on repeated line tracking and its application to personal identification - N. Miura, A. Nagasaka, and T. Miyatake ,2004
- [5]. Extraction of finger-vein patterns using maximum curvature points in image profiles - N. Miura, A. Nagasaka, and T. Miyatake,2005.
- [6]. Human identification using knucklecodes - A. Kumar and Y. Zhou ,2009.
- [7]. Personal recognition using hand-shape and texture - A. Kumar and D. Zhang ,2006.
- [8]. Pores and ridges: High resolution fingerprint matching using level 3 features - A.K. Jain, Y. Chen, and M. Demirkus ,2007.